

Probing non-thermal density fluctuations in the one-dimensional Bose gas

Jacopo De Nardis¹, Milosz Panfil², Andrea Gambassi³, Leticia F. Cugliandolo⁴, Robert Konik⁵ and Laura Foini⁶

¹ Département de Physique, École Normale Supérieure, PSL Research University, CNRS, 24 rue Lhomond, 75005 Paris, France

² Institute of Theoretical Physics, University of Warsaw, ul. Pasteura 5, 02-093 Warsaw, Poland

³ SISSA — International School for Advanced Studies and INFN, via Bonomea 265, 34136 Trieste, Italy

⁴ Sorbonne Universités, Université Pierre et Marie Curie — Paris 6, Laboratoire de Physique Théorique et Hautes Energies, 4, Place Jussieu, 75252 Paris Cedex 05, France

⁵ CMPMS Division, Brookhaven National Laboratory, Building 734, Upton, New York 11973, USA

⁶ Laboratoire de Physique Statistique, Département de l'ENS, École normale supérieure, PSL Research University, Université Paris Diderot, Sorbonne Paris Cité, Sorbonne Universités, UPMC Univ. Paris 06, CNRS, 75005 Paris, France.

E-mail: jacopo.de.nardis@phys.ens.fr

Abstract. Quantum integrable models display a rich variety of non-thermal excited states with unusual properties. The most common way to probe them is by performing a quantum quench, i.e., by letting a many-body initial state unitarily evolve with an integrable Hamiltonian. At late times, these systems are locally described by a generalized Gibbs ensemble with as many effective temperatures as their local conserved quantities. The experimental measurement of this macroscopic number of temperatures remains elusive. Here we show that they can be obtained by probing the dynamical structure factor of the system after the quench and by employing a generalized fluctuation-dissipation theorem that we provide. Our procedure allows to completely reconstruct the stationary state of a quantum integrable system from state-of-the-art experimental observations.

1. Introduction

Motivated by the impressive experimental progress in engineering and manipulating cold atomic gases, the dynamics of isolated quantum many-body systems has recently been the subject of very intense theoretical [1–3] and experimental [4–9] investigations.

In particular, it has been firmly established that the nature of the eventual statistical description of the local properties of these systems in their stationary states depends crucially on them being integrable or not. In the former case, the presence of an extensive amount of (quasi-) local quantities Q_n which are conserved by the unitary dynamics with Hamiltonian H , i.e., $[H, Q_n] = 0$, makes the system relax locally towards the generalized Gibbs ensemble (GGE) with density operator ρ_{GGE} [10–25]. The GGE also holds at intermediate times in the case of a weak integrability breaking term [4, 9, 26–31]. In the non-integrable case, instead, the relaxation generically occurs towards the Gibbs ensemble (GE) ρ_{GE} , controlled solely by H [29, 32, 33]. Both ensembles are characterized by certain parameters, which are essentially determined by the expectation values of the conserved charges.

In the Gibbs ensemble, the only relevant parameter is the temperature β^{-1} (and, possibly, the chemical potential μ in the grand canonical ensemble), which plays a fundamental role, as it completely determines the statistical and thermodynamic properties of the ensemble ρ_{GE} . Accordingly, it is very important to be able to measure the temperature. This can be done, for example, by weakly coupling the system to a thermometer or, alternatively, by studying the relationship between the measurable fluctuations occurring in the system and its response to external perturbations. The second approach relies on the so-called fluctuation-dissipation theorem (see, for example, Refs. [34–36]).

In the generalized Gibbs ensemble ρ_{GGE} , the number of parameters playing the role of “generalized temperatures” which are necessary to characterize it completely is, in principle, extensively large: the task of fixing all of them would therefore appear impractical. However, it has been recently shown [13, 37, 38] that, for a number of systems which are represented by *non-interacting* integrable models, it is possible to identify some “natural” observables, the correlations and responses of which can be used to determine the complete set of generalized temperatures *via* the corresponding fluctuation-dissipation ratios. In the presence of interactions, the analysis of integrable models becomes significantly more complex and it is therefore unclear, *a priori*, whether this approach carries over to interacting integrable models. In this work we show that this is actually the case, as the fluctuation-dissipation ratios (or, equivalently, the dynamic structure factor of the relevant fluctuations) can be used to infer all the parameters which determine ρ_{GGE} . In particular, we focus on the one-dimensional Bose gas described by the Lieb-Liniger model [39, 40] and we use the dynamical structure factor (DSF) $S(k, \omega)$, recently studied in Refs. [41, 42], in order to characterize ρ_{GGE} . This approach is remarkably useful, as it provides a viable and concrete way of measuring ρ_{GGE} in experiments with cold atoms, in which integrability breaking terms can be

controlled and made small [4, 9, 43, 44]. Moreover, we show that the fluctuation-dissipation ratio is an optimal tool to check the extent to which a system is thermalized in any experimental setting, even when the underlying model is not integrable.

Concretely, in this work we consider a quantum quench of the Lieb-Liniger Bose gas from a generic initial state $|\Psi_0\rangle$ satisfying cluster decomposition property [45]. At late times, local observables (namely those represented by operators having a support only on a finite region of the whole system) are described by a GGE reduced density matrix ρ_{GGE} . We focus here on the dynamical correlation function of the density fluctuations, namely the dynamical structure factor computed on the time-evolved initial state. As we define the time evolved expectation value of a generic local operator O as $\langle O(t) \rangle \equiv \langle \Psi_0 | e^{iHt} O e^{-iHt} | \Psi_0 \rangle$, the dynamical structure factor reads

$$S_t(k, \omega) = \int_{-\infty}^{+\infty} dt' \int dx e^{i(kx - t'\omega)} \left[\langle \rho(x, t+t') \rho(0, t) \rangle - \langle \rho(x, t+t') \rangle \langle \rho(0, t) \rangle \right] \quad (1)$$

where $\rho(x, t)$ is the density operator measuring the number of particles at position x and time t . We will show further below how its expectation value $S(k, \omega) = \lim_{t \rightarrow \infty} S_t(k, \omega)$ at late times after the quench can be used to completely reconstruct the GGE density matrix and, in particular, its effective temperatures and chemical potential, see Fig. 1. Note that, despite the presence of the integration over x in Eq. (1), the observable $S_t(k, \omega)$ is actually local for finite values of k and for all initial states $|\Psi_0\rangle$ that respect cluster decomposition property. This indeed implies that $\langle \rho(x, t+t') \rho(0, t) \rangle \rightarrow \langle \rho(x, t+t') \rangle \langle \rho(0, t) \rangle$ at large x , which effectively restricts the integral in Eq. (1) to a finite interval.

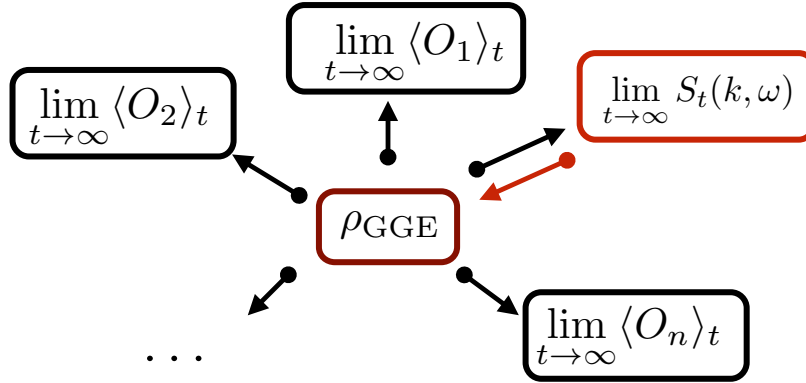


Figure 1. A GGE steady state ρ_{GGE} determines (black arrows) the expectation value of any local operator O_i in the long time limit and, in particular, also the dynamical structure factor $\lim_{t \rightarrow \infty} S_t(k, \omega)$. Here we show that, given the dynamical structure factor in the long time limit after the quench, one can use its behavior at small momentum $k \rightarrow 0$ to fully reconstruct the GGE steady state (reversed red arrow) and, thus, the expectation value of any other local operator in the same stationary state.

The manuscript is organized as follows. In Sec. 2 we explain our approach in a generic setting. In Secs. 3 and 4 we focus on the one dimensional Bose gas as described

by the Lieb-Liniger model with no confining potential and we detail how our approach applies to this problem. Specifically, in Sec. 4 we focus on the case of an interaction quench from the BEC initial state. Finally, in Sec. 5 we present conclusions and perspectives. Some details of the analysis are reported in [Appendix A](#) and [Appendix B](#). In [Appendix C](#) we discuss an alternative approach to determining the GGE, which is valid in the strongly interacting regime of the Lieb-Liniger model. In [Appendix D](#) and [Appendix E](#) we discuss possible experimental issues in implementing the proposed protocol and how to cope with them. In [Appendix F](#) we comment on the ABACUS [46] software package that we used for numerical evaluation of the dynamical structure factor.

2. Generalized temperatures in integrable models

Integrable models are generically characterized by *interacting* quasi-particles, i.e., by stable collective thermodynamic excitation modes which, due to their interactions, undergo elastic (non-diffractive) scattering. In the absence of interactions and in systems which are invariant under space translations, these modes can be labeled by their momentum k . Analogously, in the presence of an integrable interaction, each excitation mode can be labeled by a quasi-momentum or rapidity λ (where $\lambda \in \mathbb{R}$ parametrizes the corresponding actual momentum $k(\lambda)$) and the type of the excitation. Focussing on the case where only one type of excitation is present (as it happens in the one-dimensional Bose gas) each eigenstate of the many-body Hamiltonian H can be formally specified by a single macroscopic mode occupation number $\vartheta(\lambda) \in [0, 1]$, defined as the fraction of the possible modes actually occupied within the rapidity interval $[\lambda, \lambda + d\lambda)$ of infinitesimal width $d\lambda$.

At thermal equilibrium within the (grand canonical) Gibbs ensemble $\rho_{\text{GE}} = e^{-\beta(H-\mu N)}$ with temperature β^{-1} and chemical potential μ , this function $\vartheta(\lambda)$ is given by [47]

$$\vartheta(\lambda) = \vartheta_{\text{GE}}(\lambda) \equiv \frac{1}{1 + e^{\beta(\omega(\lambda)-\mu)}} , \quad (2)$$

i.e., by the Fermi distribution in terms of the excitation energy $\omega(\lambda)$ (c.f. Eq. (16)) of the mode λ .

Thermal states are not the only excited states that one can typically observe in an integrable model. In order to realize a non-thermal state a convenient protocol consists in preparing the system in a certain initial state $|\Psi_0\rangle$ which is not an eigenstate of the Hamiltonian H , and let it evolve under a unitary time evolution $|\Psi_0(t)\rangle = e^{-itH}|\Psi_0\rangle$ until a *local* stationary state is reached. As indeed anticipated in the introduction, though the ensuing evolution is unitary and the evolved state is a pure state, the long-time limit of the expectation value $\langle O \rangle_t$ of any local observable O can actually be described by an equivalent statistical ensemble. For an integrable H in the thermodynamic limit, this is thought to be given by the generalized Gibbs ensemble ρ_{GGE} as originally introduced

in Refs. [10]

$$\lim_{t \rightarrow \infty} \langle O \rangle_t = \text{tr}[\rho_{\text{GGE}} O] \quad \text{with} \quad \rho_{\text{GGE}} = \frac{e^{-\sum_n \mu_n Q_n}}{\text{tr}[e^{-\sum_n \mu_n Q_n}]}, \quad (3)$$

where $\{Q_n\}_n$ is the set of local or quasi-local conserved quantities and $\{\mu_n\}_n$ are the associated Lagrange multipliers. The values of these multipliers depend on the initial state $|\Psi_0\rangle$ of the evolution, as they are fixed by the very fact that each Q_n is conserved by the dynamics and their statistical average over ρ_{GGE} has to be equal to their initial value, i.e.,

$$\langle \Psi_0 | Q_n | \Psi_0 \rangle = \text{tr}[\rho_{\text{GGE}} Q_n] \quad (4)$$

for each charge Q_n . This approach based on focussing on the emerging statistical ensemble is appealing from the theoretical point of view, as it involves the conserved charges Q_n , which generically play a primary role in integrable models.

However, in the quench that we focus on in this paper, the expectation values of these charges are not well defined because of various ultra-violet divergences [48–51]. Accordingly, instead of using them to construct the GGE ensemble we define it via the macroscopic distribution $\vartheta(\lambda) \equiv \vartheta_{\text{GGE}}(\lambda)$ of the occupied modes after the quench, employing the micro-canonical GGE formulation [52–54] where the trace over the Hilbert space in Eq. (3) can be expressed as the expectation value on a single eigenstate $|\vartheta_{\text{GGE}}\rangle$ of the model characterized by the mode occupation $\vartheta_{\text{GGE}}(\lambda)$, i.e.,

$$\lim_{t \rightarrow \infty} \langle O \rangle_t = \langle \vartheta_{\text{GGE}} | O | \vartheta_{\text{GGE}} \rangle. \quad (5)$$

This is fully analogous to the case of thermal equilibrium, where the eigenstate thermalization hypothesis [32, 33] allows one to compute expectation values at thermal equilibrium for a generic quantum state in terms of a single eigenstate. For later convenience we parameterize $\vartheta_{\text{GGE}}(\lambda)$ in terms of a function $\epsilon(\lambda)$ as

$$\vartheta_{\text{GGE}}(\lambda) = \frac{1}{1 + e^{\epsilon(\lambda)}}. \quad (6)$$

Motivated by the case of thermal equilibrium in Eq. (2), we rewrite $\epsilon(\lambda)$ as the (unique) product

$$\epsilon(\lambda) = \beta(\lambda) [\omega(\lambda) - \bar{\mu}] \quad (7)$$

of a mode-dependent inverse “effective temperature” $\beta(\lambda)$ and the mode energy $\omega(\lambda)$. The effective chemical potential $\bar{\mu}$ is defined by requiring that $\epsilon(\lambda)$ vanishes at $\lambda = \bar{\lambda}_F$, i.e.,

$$\bar{\mu} = \omega(\bar{\lambda}_F), \quad (8)$$

where $\bar{\lambda}_F$ generalizes the equilibrium Fermi mode out of equilibrium, with $\vartheta_{\text{GGE}}(\bar{\lambda}_F) = 1/2$. Note that, due to the interactions among the excitations, the mode energy $\omega(\lambda)$ in Eq. (7), defined in Eq. (16), is itself a non-trivial functional of $\vartheta(\lambda)$ and therefore of $\beta(\lambda)$ via Eq. (6).

We emphasize that the effective temperatures $\beta^{-1}(\lambda)$ and the chemical potential $\bar{\mu}$ are not the Lagrange parameters $\{\mu_n\}_n$ introduced in Eq. (3) for the one-dimensional Bose gas, although they can be related to them by expanding the function $\epsilon(\lambda)$ on the basis of the eigenvectors of a particular set of charges $\{Q_n\}_n$. For example, if for the charges $\{Q_n\}$ we choose the set of quasi-local charges $\{I_\alpha^{(-)}, I_\alpha^{(+)}\}_\alpha$ introduced in [50, 51] with single-particle eigenvalues $\{\sin(\alpha\lambda), \cos(\alpha\lambda)\}_\alpha$ for any real α we have

$$\epsilon(\lambda) = \int_{-\infty}^{+\infty} d\alpha [\mu_\alpha^{(-)} \sin(\alpha\lambda) + \mu_\alpha^{(+)} \cos(\alpha\lambda)]. \quad (9)$$

Finally, once we have determined the distribution $\vartheta_{\text{GGE}}(\lambda)$ for a given initial state, we can then rewrite any expectation value at long times after the quench as an expectation value on this single eigenstate of the model, as done in Eq. (5) and analogously to what was done in [19, 49, 52, 55].

The approach we pursue here, which was introduced in Ref. [38], consists in a direct measurement of $\vartheta_{\text{GGE}}(\lambda)$ in Eq. (6), based on the knowledge of the DSF $S_t(k, \omega)$ long after the quench. From this function $\vartheta_{\text{GGE}}(\lambda)$, we can then determine any other expectation value of local operators in the long time limit. Although the approach outlined here is applicable to a generic system described by an integrable model and, in principle, to a generic initial state $|\Psi_0\rangle$ which fulfills the cluster decomposition propriety, below we focus on the one-dimensional Bose gas (i.e., on the so-called Lieb-Liniger model), for which the expression of the DSF $S(k, \omega)$ at low momenta and for a generic macroscopic state $|\vartheta\rangle$ has been recently calculated analytically in Ref. [41]. For simplicity, in Secs. 3 and 4 we consider the case in which no external confining potential is applied to the gas, while more realistic experimental conditions which involve, e.g., the presence of an harmonic trap are discussed in Appendix D and Appendix E.

3. From the dynamic structure factor of the one-dimensional Bose gas to the steady state

3.1. The Lieb-Liniger model

The Hamiltonian H of a Bose gas consisting of N particles in one spatial dimension (Lieb-Liniger model) [39, 40] is

$$H = - \sum_{i=1}^N \partial_{x_i}^2 + 2c \sum_{i>j}^N \delta(x_i - x_j), \quad (10)$$

where x_i denotes the position of the i -th particle, c measures the strength of their repulsive contact interaction, and the units of measure are chosen such that $\hbar^2/2m = 1$. The model can be realized experimentally on atom chips and optical lattices and in the past years many of its equilibrium properties have been studied in great detail [43, 44, 56–58]. We consider the gas to be confined within a finite segment of length L , with periodic boundary conditions (we consider the effect of a possible harmonic

trap in [Appendix D](#)). The effective interaction is characterized by the dimensionless parameter $\gamma = c/n$, where $n = N/L$ is the linear particle density of the gas. In the thermodynamic limit $L \rightarrow \infty$ with fixed n (or, alternatively with fixed chemical potential μ), the eigenstates of H , referred to as Bethe states, are labeled by the filling function $\vartheta(\lambda) \in [0, 1]$ which is the fraction of occupied modes within the interval $[\lambda, \lambda + d\lambda)$. Once the filling function $\vartheta(\lambda)$ is specified, the relevant thermodynamic quantities which characterize the state of the system can be easily determined [\[47\]](#). For example, the total particle density n and the energy density e can be expressed in terms of the filling function and the total density of modes $\rho_t(\lambda)$

$$n = \int_{-\infty}^{+\infty} d\lambda \vartheta(\lambda) \rho_t(\lambda), \quad (11)$$

and

$$e = \int_{-\infty}^{+\infty} d\lambda \lambda^2 \vartheta(\lambda) \rho_t(\lambda), \quad (12)$$

respectively. In the case $c = \infty$ of hard-core bosons, the maximal number $2\pi\rho_t(\lambda)d\lambda$ of allowed modes within the interval $[\lambda, \lambda + d\lambda)$ is identically equal to 1. When c is finite $\rho_t(\lambda)$ becomes a non-trivial function as the inter-particle interactions affect the modes, which are no longer homogeneously distributed in the space of rapidities. The total density $\rho_t(\lambda)$ of possible states and their actual occupation $\vartheta(\lambda)\rho_t(\lambda)$ are related by an integral equation [\[47\]](#)

$$2\pi\rho_t(\lambda) = 1 + \int_{-\infty}^{+\infty} d\lambda' K(\lambda - \lambda') \vartheta(\lambda') \rho_t(\lambda'), \quad (13)$$

where the so-called scattering kernel is given by

$$K(\lambda) = \frac{2c}{\lambda^2 + c^2}. \quad (14)$$

As a consequence of the interaction, the total density ρ_t of modes at a certain rapidity λ is influenced by the occupation $\vartheta(\lambda')$ of those with rapidity λ' , weighted by the kernel $K(\lambda - \lambda')$.

3.2. Excitations of a macroscopic state

In order to study correlation functions, it is important to understand the structure of the excitations of a macroscopic state $|\vartheta\rangle$ of the system, which is specified by a certain occupation function $\vartheta(\lambda)$, see Refs. [\[41, 42\]](#). If the system is confined within a finite “volume” L , a single particle excitation corresponds to increasing by one the occupation number of a certain mode with quasi-momentum p . The resulting momentum $k(p)$ and excitation energy $\omega(p)$ can be expressed, in the thermodynamic limit, as

$$k(p) = p - \int_{-\infty}^{+\infty} d\lambda \vartheta(\lambda) F(\lambda|p), \quad (15)$$

$$\omega(p) = p^2 - 2 \int_{-\infty}^{+\infty} d\lambda \lambda \vartheta(\lambda) F(\lambda|p), \quad (16)$$

where we introduced the so-called back-flow function $F(\lambda|p)$ which describes the effects of the excitation on the occupation of the remaining modes, as schematically shown in Fig. 2. This function turns out to satisfy [47]

$$2\pi F(\lambda|p) = \theta(\lambda - p) + \int_{-\infty}^{\infty} d\lambda' K(\lambda - \lambda') \vartheta(\lambda') F(\lambda'|p), \quad (17)$$

where

$$\theta(\lambda) = 2 \arctan(\lambda/c), \quad (18)$$

represents the scattering phase shift, related to K in Eq. (14) by $K(\lambda) = \theta'(\lambda)$. Analogously, the occupation number of a certain mode with rapidity h can be decreased

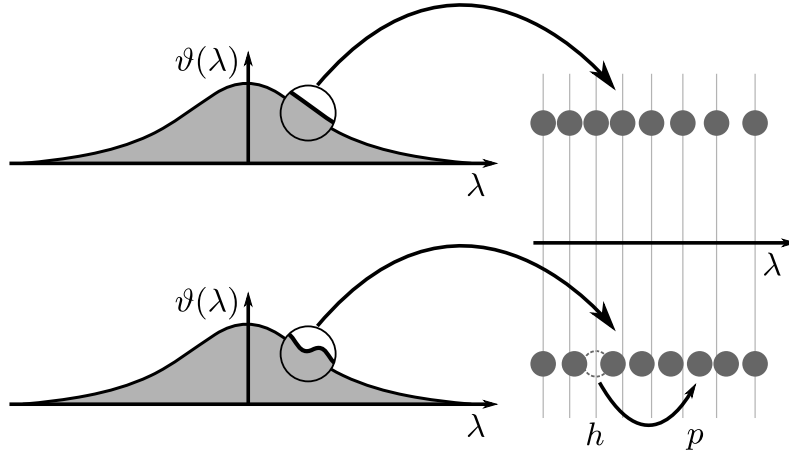


Figure 2. The filling function $\vartheta(\lambda)$, depicted on the upper part of the figure as a function of λ , describes how densely modes with different rapidities (indicated by the sequence of circles and thin vertical lines on the right, along the rapidity axis) are populated. The filling function of an excited state depicted in the lower part of the figure is macroscopically the same as the one above. However, by zooming in the region of the particle-hole excitation, indicated by the arrow on the right, reveals both a displacement of one quasi-particle from the position it was originally occupying (dashed circle) and a small shift in the (allowed) quasi-momenta of all the other particles, as indicated by the filled circles on the right. This shift compared to the original allowed rapidities (vertical lines) is described by the back-flow function $F(\lambda|p, h)$ and it contributes to the momentum and energy of the excited state as shown in Eqs. (15), (16) and (19).

by one, resulting into the creation of a hole excitation, with momentum and energy opposite to those of the corresponding particle excitation. Accordingly, a particle-hole excitation is characterized by a momentum $k(p, h)$ and an energy $\omega(p, h)$, given by

$$k(p, h) = k(p) - k(h), \quad \text{and} \quad \omega(p, h) = \omega(p) - \omega(h), \quad (19)$$

respectively.

3.3. One particle-hole kinematics at small momentum

In the small momentum limit $k \ll k_F = \pi n$, i.e., when the particle and hole are close to each other $p \simeq h$, the momentum and energy in Eq. (19) (see also Eqs. (15) and (16)) can be expressed in terms of the single particle and hole rapidities (p, h) via [41]

$$k(p, h) = 2\pi(p - h)\rho_t(h), \quad (20)$$

$$\omega(p, h) = v(h)k(p, h), \quad (21)$$

where we introduced the sound velocity $v(h)$, which depends only on the rapidity of the hole excitation via

$$v(h) = \frac{h + \int_{-\infty}^{+\infty} d\lambda \lambda L(h, \lambda)}{\pi \rho_t(h)}, \quad (22)$$

where $L(\lambda, \mu) = -\vartheta(\mu)\partial_\mu F(\lambda|\mu)$ is related to the derivative of the back-flow function and satisfies the integral equation [41]

$$L(\lambda, \lambda'') = K(\lambda - \lambda'')\vartheta(\lambda'') + \int_{-\infty}^{+\infty} d\lambda' K(\lambda - \lambda')\vartheta(\lambda')L(\lambda', \lambda''). \quad (23)$$

The velocity $v(h)$ can be both positive and negative.

3.4. The fluctuation-dissipation ratio

In order to introduce the fluctuation-dissipation ratio mentioned in the Introduction, we define the symmetrized correlation function C_+ , which corresponds to the connected expectation value of the anticommutator of the particle densities at different space-time points, i.e.,

$$\begin{aligned} C_+(x, t) &= \left\langle \frac{\rho(x, t)\rho(0, 0) + \rho(0, 0)\rho(x, t)}{2} \right\rangle - \langle \rho(0, 0) \rangle^2 \\ &= \frac{C(x, t) + C(-x, -t)}{2}, \end{aligned} \quad (24)$$

where translational invariance in both space and time has been used. Although invariance under time translation is broken by a quench, one expects to recover it in the long time stationary state. The variation of the average density $\langle \rho(x, t) \rangle$ in response to a local change at, say, point x' and time t' in the chemical potential μ (which is conjugate to the density ρ) is quantified by the response function $R(x - x', t - t')$, which, via the Kubo relation [34], can be expressed as the expectation value of the commutator

$$R(x, t) = iu(t)\langle [\rho(x, t), \rho(0, 0)] \rangle, \quad (25)$$

where $u(t < 0) = 0$ and $u(t > 0) = 1$ is the Heaviside function. Using the following definition of the Fourier transform $f(\omega, t)$ of a function $f(x, t)$,

$$f(k, \omega) = \int dx \int_{-\infty}^{+\infty} dt e^{i(kx - \omega t)} f(x, t), \quad (26)$$

one can easily show that

$$\text{Im } R(k, \omega) = \frac{S(k, \omega) - S(k, -\omega)}{2}, \quad (27)$$

where $S(k, \omega)$ is the DSF, i.e., the Fourier transform of the density-density correlations $C(x, t) = C(-x, t) = \langle \rho(x, t) \rho(0, 0) \rangle - \langle \rho(0, 0) \rangle^2$ in the stationary state.

In the grand canonical equilibrium with density matrix $\rho_{\text{GE}} = e^{-\beta(H - \mu N)}$, the cyclic property of the trace implies the fluctuation-dissipation theorem [34], i.e.,

$$S(k, -\omega) = e^{-\beta\omega} S(k, \omega); \quad (28)$$

this equality establishes a sort of universal relationship between the correlation and response functions introduced above, better expressed by the fact that their fluctuation-dissipation ratio (FDR) [36, 59]

$$\Xi(k, \omega) \equiv \frac{\text{Im } R(k, \omega)}{C_+(k, \omega)} = \frac{S(k, \omega) - S(k, -\omega)}{S(k, \omega) + S(k, -\omega)} = \tanh(\beta\omega/2), \quad (29)$$

as a consequence of Eq. (28). Accordingly, by determining the FDR $\Xi(k, \omega)$ one can infer the temperature β^{-1} of the system only on the basis of dynamical quantities which can in principle be measured in an experiment.

3.5. Determining $\vartheta_{\text{GGE}}(\lambda)$ from a generalized fluctuation-dissipation ratio

In Ref. [38] it was argued that for those integrable systems which can be mapped onto non-interacting models, the FDR in Eq. (29) can actually be used to extract the GGE effective temperatures $\beta(\lambda)^{-1}$. Here we show that this observation generalizes to interacting integrable models. Our approach reads as follows: given an initial condition, we measure the correlation and response functions long after the quench and, either from their ratio Ξ or directly from the DSF, we infer the distribution ϑ_{GGE} .

In order to do so we need a relationship between $\Xi(k, \omega)$ and $\vartheta(\lambda)$. It was established in Ref. [41] that at small momentum $k \ll k_F$ a generalized formulation of the fluctuation-dissipation theorem (29) holds. For the present purpose an additional reformulation of this relation is needed and in Appendix A we prove that it reads

$$\Xi(k, \omega) = \tanh \left(\frac{k}{2} \frac{\partial_\lambda \epsilon(\lambda)}{2\pi \rho_t(\lambda)} \right) \Big|_{\lambda=\lambda(k, \omega)} + \mathcal{O}(k^2), \quad (30)$$

where $\rho_t(\lambda)$ is given in Eq. (13) in terms of $\vartheta(\lambda)$. This equation follows from the fact that a perturbation with small momentum $k \ll k_F$ but arbitrary energy ω can only create a single particle-hole excitation, while multiple particle-hole excitations require probing fluctuations and perturbations with larger momenta. The value $\lambda(k, \omega)$ of the rapidity at which the r.h.s. of Eq. (30) is evaluated is fixed by the relationship (21) between the energy and momentum of the relevant single particle-hole excitation and it is therefore such that

$$v(\lambda(k, \omega)) = \omega/k, \quad (31)$$

with the sound velocity v given by Eq. (22).

In order to find $\vartheta(\lambda) = [1 + e^{\epsilon(\lambda)}]^{-1}$ we invert Eq. (30), we integrate and we neglect all the corrections due to finite k by taking the limit $k \rightarrow 0$:

$$\log \left(\frac{1 - \vartheta(\lambda)}{\vartheta(\lambda)} \right) = \lim_{k \rightarrow 0} \left(\frac{2}{k} \int^\lambda d\lambda' 2\pi \rho_t(\lambda') \operatorname{arctanh} \Xi(k, k v(\lambda')) + \text{const.} \right). \quad (32)$$

This expression can also be conveniently re-written as an integral over the energies ω by using Eq. (31)

$$\log \left(\frac{1 - \vartheta(\lambda)}{\vartheta(\lambda)} \right) = \lim_{k \rightarrow 0} \left(\frac{2}{k^2} \int^{kv(\lambda)} d\omega 2\pi \frac{\rho_t(\lambda(k, \omega))}{v'(\lambda(k, \omega))} \operatorname{arctanh} \Xi(k, \omega) + \text{const} \right), \quad (33)$$

where $v'(\lambda)$ indicates the derivative of $v(\lambda)$ and $\lambda(k, \omega)$ is given by Eq. (31).

Our protocol to determine $\vartheta(\lambda) = \vartheta_{\text{GGE}}(\lambda)$ after a quantum quench is as follows: given the DSF $S(k, \omega) = \lim_{t \rightarrow \infty} S_t(k, \omega)$ (see Eq. (1)) at late times after the quench, the integrals in Eq. (32) or (33) can be computed once the total density $\rho_t(\lambda)$ and the sound velocity $v(\lambda)$ are known. We note that $\rho_t(\lambda)$ and $v(\lambda)$ are given by integral equations depending on $\vartheta(\lambda)$ (see Eq. (13) for ρ_t and Eqs. (22) and (23) for $v(\lambda)$) and therefore Eq. (32) or (33) have to be computed iteratively on ϑ . Moreover, also the remaining integration constant in Eqs. (32) and (33) has to be fixed iteratively by imposing that the density of the gas calculated according to Eq. (11) matches its actual value. Note that although the equivalence in Eqs. (32) and (33) holds only in the limit $k \rightarrow 0$, the finite k corrections are of $\mathcal{O}(k^2)$ as in Eq. (30), which makes then possible to compute $\vartheta(\lambda)$ also by using the DSF at small but finite values of k .

4. Application to the quench from the BEC state

In order to demonstrate the applicability of Eq. (32) (or, equivalently, Eq. (33)) for determining ϑ_{GGE} after a quantum quench on the basis of the knowledge of the DSF $S_t(k, \omega)$ (see Eq. (1)) in the large time limit we “simulate” a particular quantum quench and we compute $S_t(k, \omega)$ numerically in the stationary state. In particular, we prepare the gas in the spatially homogeneous ground state $|\Psi_0\rangle$ of the Hamiltonian H in Eq. (10) with $c = 0$ (the so-called BEC state) and density $n = 1$, with $N = L = 20$ and we let it evolve with the same Hamiltonian but with $c \neq 0$. For this quench the overlaps $\langle \Psi_0 | \alpha \rangle$ between the initial state $|\Psi_0\rangle$ and the eigenstates $|\alpha\rangle$ of H with non-vanishing c are known [60] and, accordingly, we can follow the evolution from the initial state and access the eventual GGE as time goes by. We consider the density-density correlations on the time-evolved initial state

$$C_t(x, t') = \langle \Psi_0 | \rho(x, t + t') \rho(0, t) | \Psi_0 \rangle - n^2, \quad (34)$$

(where we used the fact that the initial state is homogeneous at all times and therefore $\langle \Psi_0 | \rho(x, t) | \Psi_0 \rangle = n$) and consider the DSF $S_t(k, \omega)$ obtained from its Fourier transform

with respect to the space and time-delay t' , with fixed t , according to Eq. (26) (see also Eq. (1)). Inserting twice the resolution of the identity

$$1 = \sum_{\alpha \in \text{span}(H)} |\alpha\rangle\langle\alpha|, \quad (35)$$

in terms of the (Bethe) eigenstates $\{|\alpha\rangle\}$ of the post-quench Hamiltonian H with eigenvalues $\{E_\alpha\}$, the DSF can be written as

$$S_t(k, \omega) = \sum_{\alpha, \beta} \langle\alpha|\Psi_0\rangle\langle\Psi_0|\beta\rangle e^{-it(E_\alpha - E_\beta)} S_{\alpha, \beta}(k, \omega), \quad (36)$$

where $S_{\alpha, \beta}(k, \omega)$ is the DSF determined between the Hamiltonian eigenstates $|\alpha\rangle$ and $|\beta\rangle$, i.e., the Fourier transform of $\langle\beta|\rho(x, t')\rho(0, 0)|\alpha\rangle - n^2$ (with $n = 1$ in this specific quench). While, in principle, we could calculate the DSF of the density fluctuations in the GGE by letting $t \rightarrow \infty$ in Eq. (36), we actually assume that one can access $S_t(k, \omega)$ only up to a moderately long time T (with respect to the typical relaxation time scale of the system, see Appendix D), as it is the case both in experimental realizations and in numerical calculations. We then approximate the actual asymptotic DSF $S(k, \omega) \equiv S_{t \rightarrow \infty}(k, \omega)$ with the one obtained by averaging $S_t(k, \omega)$ over time, in order to average out possible oscillations:

$$\bar{S}_T(k, \omega) = \frac{1}{T} \int_0^T dt S_t(k, \omega). \quad (37)$$

In the limit of large T , \bar{S}_T becomes identical to the density-density correlation in the GGE up to finite-size corrections and it can actually be expressed as an average over the so-called diagonal ensemble [33]

$$S(k, \omega) \equiv \lim_{T \rightarrow \infty} \bar{S}_T(k, \omega) = \sum_{\alpha} |\langle\alpha|\Psi_0\rangle|^2 S_{\alpha, \alpha}(k, \omega). \quad (38)$$

In Appendix E we discuss how this quantity can in principle be measured in experiments. In the next subsection, instead, we proceed to its numerical computation based on the ABACUS code [46, 61–63] (see also Appendix F) which allows us to determine the r.h.s. of Eq. (38) and extract, as explained in the previous subsection, the numerical estimate ϑ_{num} of the distribution ϑ . Then, ϑ_{num} can be compared with the exact ϑ_{GGE} , analytically determined in Ref. [60] for this particular quench and which can be written as

$$\vartheta_{\text{GGE}}(\lambda) = \frac{a(\lambda)}{1 + a(\lambda)}, \quad (39)$$

with the function $a(\lambda)$ given by

$$a(\lambda) = \frac{2\pi/\gamma}{(\lambda/c) \sinh(2\pi\lambda/c)} \left| I_{1 \pm 2i(\lambda/c)}(4/\sqrt{\gamma}) \right|^2, \quad (40)$$

where $I_\alpha(z)$ is the modified Bessel function of the first kind and $\gamma = c/n$. The corresponding effective temperatures $\beta(\lambda)$ can now be easily calculated by using Eq. (7)

with $\epsilon(\lambda) = -\ln a(\lambda)$ (see Eq. (6)) and $\omega(\lambda)$ given by Eq. (16). Figure 3 and 4 show the inverse effective temperatures $\beta(\lambda)$ and the effective chemical potential $\bar{\mu}$ for quenches from the BEC state to different values of the couplings, parametrized by different values of $c = \gamma$ (we recall that we have choose unitary density of the gas $n = 1$).

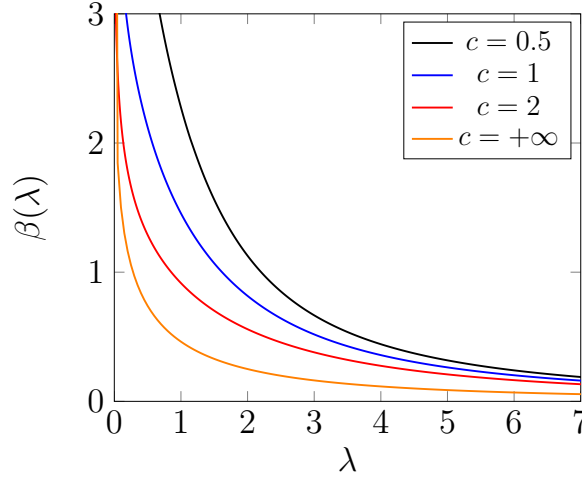


Figure 3. Dependence of the inverse effective temperatures $\beta(\lambda)$ on the rapidity λ for four quenches from the BEC state to the interacting theory with coupling $c = 0.5, 1, 2, +\infty$ (from top to bottom with $n = 1$), as obtained from the exact $\vartheta(\lambda)$ reported in Eq. (39). Note that $\beta(\lambda)$ diverges as $\log \lambda^2$ at small λ , signaling that the distribution at small rapidities is effectively as that in the ground state of the model, while these inverse temperatures vanish at large λ , indicating that these modes are highly populated as a result of the quench.

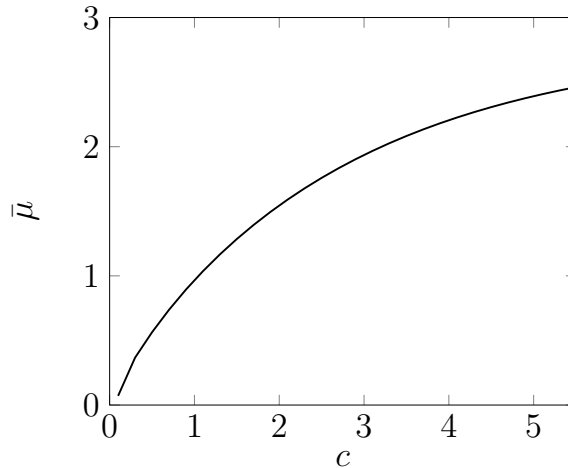


Figure 4. Dependence of the effective chemical potential $\bar{\mu}$ on the final value of the interaction c . At large c , $\bar{\mu}$ asymptotically approaches the analytically predicted value $\bar{\mu} \rightarrow 4$ (see Appendix B) while it vanishes for small c (shallow quench limit) as expected for the BEC state (ground state of free bosons).

4.1. Numerical results

Figure 5 shows the dependence of the DSF $S(k, \omega)$ on the frequency ω within the range $|\omega| \leq 3\omega_F$, where $\omega_F = k_F^2 = \pi^2 n^2$ is the Fermi energy and for three values of the wave-vector $k = 0.2k_F, 0.4k_F, 0.6k_F$. In particular, the curves on the left panel are calculated numerically with the ABACUS code ($N = L = 20$) after the quench to $c = 2$, while those on the right panel correspond to the analytic expressions which can be obtained in the thermodynamic limit with $n = 1$ and $c \rightarrow \infty$ as briefly discussed in Appendix B.

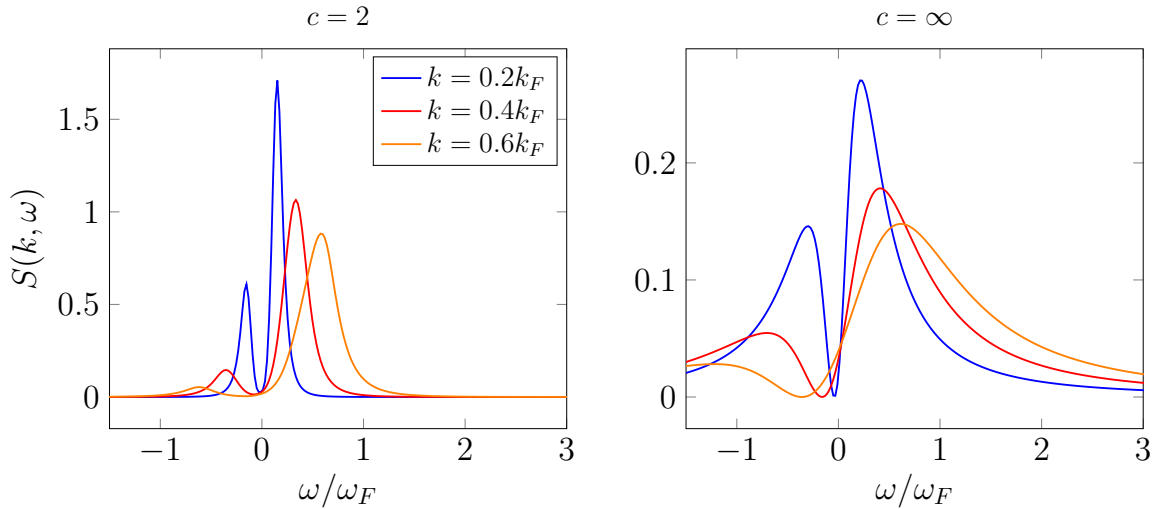


Figure 5. Dependence of the dynamic structure factor $S(k, \omega)$ of the post-quench diagonal ensemble (38) on the frequency ω/ω_F with the Fermi energy $\omega_F = k_F^2$, for three values of the wave-vector $k = 0.2k_F, 0.4k_F$, and $0.6k_F$. The left and the right panels correspond to a quench to $c = 2$ and $c \rightarrow \infty$, respectively. In the left panel the curves are obtained via a numerical computation with the ABACUS code for $N = L = 20$ and $c = 2$ while in the right panel the curves correspond to the analytic prediction for the case $c \rightarrow \infty$ in the thermodynamic limit $N \rightarrow \infty, L \rightarrow \infty$ with $n = 1$, derived in Ref. [64].

Based on the numerical data for $S(k, \omega)$ reported on the left panel of Fig. 5 — which mimic the result of a possible scattering experiment discussed in Appendix E — we can now use Eq. (32) in order to extract the numerical estimate ϑ_{num} of the distribution ϑ for a quench from the BEC state to $c = 2$, with density $n = 1$. The resulting ϑ_{num} is reported in Fig. 6 as an even function of the rapidity λ , for two values of the wave-vector k which the data of $S(k, \omega)$ refer to. The solid line, instead, corresponds to the exact expression of ϑ which follows from Eqs. (39) and (40). The agreement between the two numerical estimates ϑ_{num} and ϑ is remarkably good and discrepancies are barely visible on this scale. Note also that while Eq. (32) is actually valid for $k \ll k_F$, the dependence of ϑ_{num} on k is practically irrelevant up to the largest value of k considered here. We point out that the numerical estimate ϑ_{num} also allows to distinguish between the GGE distribution and its thermal approximations, the GE distribution ϑ_{GE} where

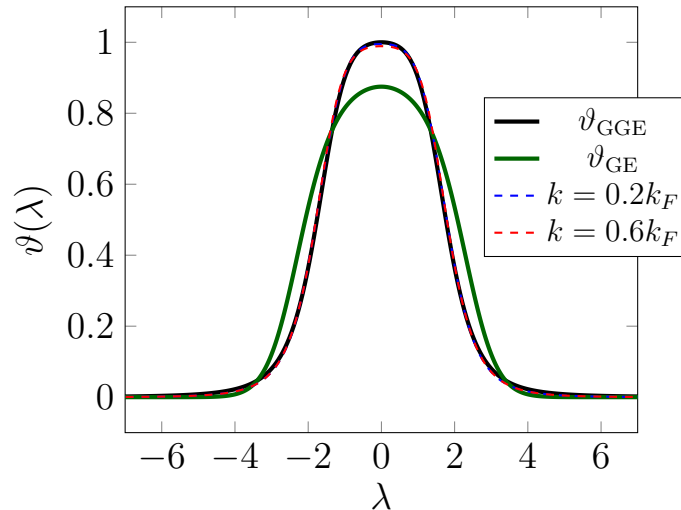


Figure 6. Comparison between the distributions $\vartheta_{\text{num}}(\lambda)$ (dashed lines) inferred via Eq. (32) on the basis of the knowledge of the dynamic structure factor $S(k, \omega)$ (with $k = 0.2k_F$ and $0.6k_F$, see the left panel in Fig. 5) and the exact $\vartheta_{\text{GGE}}(\lambda)$ given in Eqs. (39) and (40) at $c = 2$ and $n = 1$ and its correspondent thermal distribution $\vartheta_{\text{GE}}(\lambda)$. These distributions are plotted here as functions of λ for the same quench as that one considered in Fig. 5.

only the Hamiltonian H is used as local conserved charge after the quench. Note that the deviations of the estimate ϑ_{num} based on the numerical data from the exact result are due to finite-size effects and the systematic error introduced by using a small but finite k (see also Fig. F1).

In order to determine ϑ_{num} from the fluctuation-dissipation ratio $\Xi(k, \omega)$ we use Eq. (32) (or equivalently Eq. (33)), and the relation between $\Xi(k, \omega)$ and $S(k, \omega)$ given in Eq. (29). Figure 7 shows the dependence of $\Xi(k, \omega)$ on ω , for the same three values of k , quenches and data considered in Fig. 5. In particular, the left and right panels correspond to quenches to $c = 2$ and $c \rightarrow \infty$, respectively. In the latter case (right), the curves clearly show that $\Xi(k, \omega)$ vanishes, for fixed k , as $|\omega| \rightarrow \infty$, as it was analytically shown in Ref. [64] and the same behavior is expected for any quench to $c > 0$ (left) despite the fact that numerical artifacts (due to the truncated diagonal ensemble used in order to numerically compute the dynamical structure factor as in (38)) hide it.

5. Conclusions and perspectives

In this work we have presented a method which allows one to completely determine the stationary state of a quantum integrable model from the knowledge of a dynamic structure factor. This approach is solely based on experimentally accessible observables, it characterizes the stationary state via the mode occupation numbers and, it does not rely on the knowledge of the conserved charges or their expectation values. For the

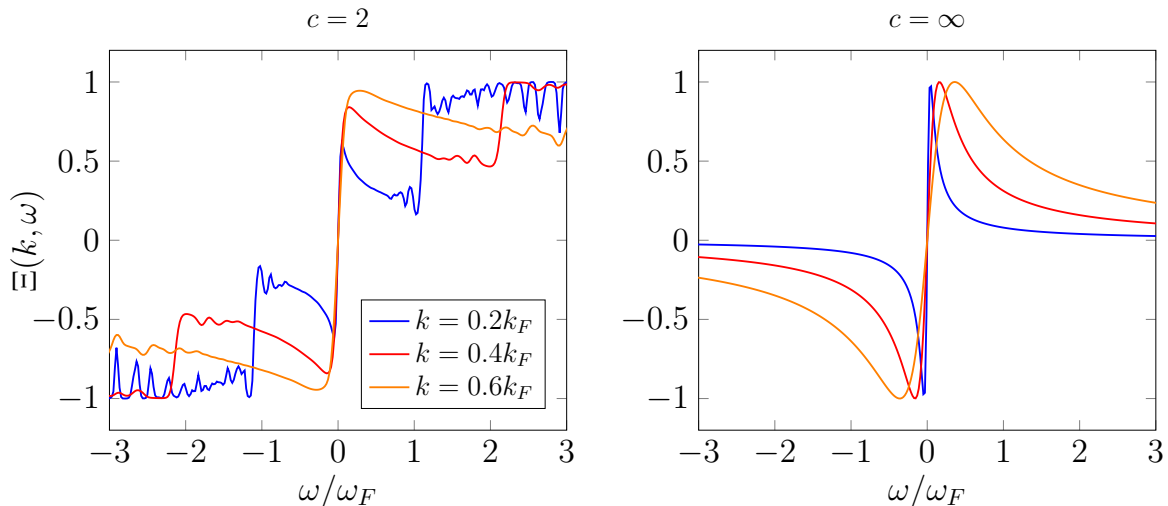


Figure 7. Dependence of the fluctuation-dissipation ratio $\Xi(k, \omega)$ on ω/ω_F with the Fermi energy $\omega_F = k_F^2$ as calculated from the post-quench diagonal ensemble (38) for the three different values of k indicated in the legend, corresponding to the same data and quenches as in Fig. 5. The left and right panels correspond to a quench to $c = 2$ and $c \rightarrow \infty$, respectively. The abrupt increase in $\Xi(k, \omega)$ at $c = 2$ (for example at $k = 0.2k_F$ around $\omega/\omega_F = \pm 1$) is a numerical artifact due to the numerical truncation of the sum over the diagonal ensemble (38).

interaction quench considered here, it circumvents the technical difficulties encountered in the direct construction of the GGE ensemble based on these charges.

In most of the experiments with ultracold atoms, the possible thermal nature of their stationary state is typically probed by measuring the momentum distribution of the atoms. However, more detailed information can be inferred from spatially or temporally resolved density correlation functions, such as those that we propose to study here. For example, the phase correlation between two halves of the gas after they have been split in space was used in Ref. [9] in order to monitor the possible thermalization of the system, while currently available experimental techniques allow the determination of structure factors via Bragg spectroscopy (see, e.g., Refs. [43, 44]). Although it has not yet been measured experimentally, we expect the post-quench time evolution of the dynamic structure factor $S(k, \omega)$ of density correlations discussed here to be within experimental reach. Our protocol allows one to extract the full steady state from simple measurements on the system: accordingly, cold atoms experiments or numerical algorithms might have access to quantities that were so far out of reach. The approach discussed here also provides a powerful method to quantify and characterize non-thermal fluctuations in a generic cold atomic gas.

An interesting open question is how to extend the analysis presented here to systems with different particle types, like the attractive Lieb-Liniger model, where different bound states of particles can coexist in the same eigenstate, or lattice models like the XXZ spin chain. Moreover, it will be interesting to test our approach in non-homogenous

non-equilibrium conditions, like the ones recently treated, e.g. in Refs. [65, 66]. Another area in which a similar analysis could apply are integrable field theories [14, 21, 67, 68]. We leave these questions open for future studies.

Acknowledgements L. F. Cugliandolo is a member of Institut Universitaire de France. We are indebted to J.-S. Caux for the use of the ABACUS software package.

Funding information JDN acknowledges support by LabEX ENS-ICFP:ANR-10-LABX-0010/ANR-10-IDEX-0001-02 PSL*. MP acknowledges financial support from the Polish National Science Centre (NCN) under FUGA grant 2015/16/S/ST2/00448. LF acknowledges support by the European Research Council under the European Union's 7th Framework Programme (FP/2007-2013/ERC Grant Agreement 307087-SPARCS). R. Konik was supported by the U.S. Department of Energy, Office of Basic Energy Sciences, under Contract No. DE-AC02-98CH10886.

Appendix A. Proof of an equivalence

In this Appendix we show that Eq. (30) follows from Eq. (102) of Ref. [41], which we refer to for the notation and the definition of the various quantities involved in the proof presented below. In particular, in Ref. [41] it was shown that, with the notations introduced in Eq. (29),

$$\Xi(k, \omega) = \tanh(\hat{\mathcal{F}}(k, \omega)/2) + \mathcal{O}(k^2), \quad (\text{A.1})$$

with $\hat{\mathcal{F}}(k, \omega)$ defined as (see Eq. (102) of Ref [41])

$$\hat{\mathcal{F}}(k, \omega) = \frac{k \partial_\lambda \epsilon_d(\lambda)}{2\pi \rho_t(\lambda)}, \quad (\text{A.2})$$

where $\lambda = \lambda(\omega, k)$ is given by Eq. (31) here, while ϵ_d is obtained by dressing the bare GGE driving term $\epsilon_0(\lambda)$

$$\epsilon_d(\lambda) = \epsilon_0(\lambda) - \int_{-\infty}^{\infty} d\lambda' \partial_\lambda \epsilon_0(\lambda') F(\lambda'|\lambda) \vartheta(\lambda'), \quad (\text{A.3})$$

with

$$\epsilon_0(\lambda) = \sum_n \mu_n \epsilon_0^{(n)}(\lambda) \quad (\text{A.4})$$

where $\epsilon_0^{(n)}(\lambda)$ is the eigenvalue of the charge Q_n on a Bethe state with a single mode $N = 1$ (also denoted with bare charge, see Ref. [41] for its definition). In order to show that Eq. (30) holds as a consequence of Eq. (A.1), we need to prove that

$$\hat{\mathcal{F}}(k, \omega) = \frac{k \partial_\lambda \epsilon(\lambda)}{2\pi \rho_t(\lambda)} \Big|_{\lambda=\lambda(k, \omega)} \quad \text{with} \quad \epsilon(\lambda) = \ln \frac{1 - \vartheta(\lambda)}{\vartheta(\lambda)}, \quad (\text{A.5})$$

i.e., we shall show that $\partial_\lambda \epsilon_d(\lambda) = \partial_\lambda \epsilon(\lambda)$. To do so one needs to prove that the two dressing relations, given a bare energy $\epsilon_0(\lambda)$ and its dressed counterpart $\epsilon(\lambda)$,

$$\epsilon(\lambda) = \epsilon_0(\lambda) + \int_{-\infty}^{\infty} \frac{d\lambda'}{2\pi} K(\lambda - \lambda') \log(1 + e^{\epsilon(\lambda')}) \quad (\text{A.6})$$

and the one given by

$$\epsilon_d(\lambda) = \epsilon_0(\lambda) - \int_{-\infty}^{\infty} d\lambda' \partial_\lambda \epsilon_0(\lambda') F(\lambda'|\lambda) \vartheta(\lambda') \quad (\text{A.7})$$

are equivalent up to a constant shift $\epsilon_d = \epsilon + \text{const}$.

Taking the derivative of (A.6) with respect to λ we obtain

$$\partial_\lambda \epsilon(\lambda) = \partial_\lambda \epsilon_0(\lambda) + \int_{-\infty}^{\infty} \frac{d\lambda'}{2\pi} K(\lambda - \lambda'') \vartheta(\lambda') \partial_\lambda \epsilon(\lambda'). \quad (\text{A.8})$$

On the other hand by doing the same to Eq. (A.7) we find

$$\partial_\lambda \epsilon_d(\lambda) = \partial_\lambda \epsilon_0(\lambda) - \int_{-\infty}^{+\infty} d\lambda' \partial_\lambda \epsilon_0(\lambda') \partial_\lambda F(\lambda'|\lambda) \vartheta(\lambda'). \quad (\text{A.9})$$

As shown in Ref. [41] one has

$$\partial_\lambda F(\lambda'|\lambda) = -L(\lambda', \lambda)/\vartheta(\lambda) = -L(\lambda, \lambda')/\vartheta(\lambda') \quad (\text{A.10})$$

Accordingly, Eq. (A.9) can be written as

$$\partial_\lambda \epsilon_d(\lambda) = \partial_\lambda \epsilon_0(\lambda) + \int_{-\infty}^{\infty} d\lambda' L(\lambda, \lambda') \partial_\lambda \epsilon_0(\lambda'), \quad (\text{A.11})$$

which, by using that $(\delta + L) = (\delta - \frac{K}{2\pi} \vartheta)^{-1}$ (where δ is the Dirac delta operator and this relation has to be understood in terms of generalized distribution functions) one finds

$$\int_{-\infty}^{+\infty} d\lambda' \left[\delta(\lambda - \lambda') - \frac{K(\lambda - \lambda')}{2\pi} \vartheta(\lambda') \right] \partial_\lambda \epsilon_d(\lambda') = \partial_\lambda \epsilon_0(\lambda), \quad (\text{A.12})$$

which is actually the same as Eq. (A.8) and therefore $\partial_\lambda \epsilon_d(\lambda) = \partial_\lambda \epsilon(\lambda)$.

Appendix B. The free limit $c \rightarrow \infty$

In the $c \rightarrow \infty$ case one has $v(\lambda) = 2\lambda$ and $2\pi\rho_t(\lambda) = 1$. From Eqs. (32) and (6) we get

$$\epsilon(\lambda) = \lim_{k \rightarrow 0} \left(\frac{2}{k} \int^\lambda d\lambda' \operatorname{arctanh} \Xi(k, k v(\lambda')) + \text{const} \right). \quad (\text{B.1})$$

The DSF $S(k, \omega)$ is known exactly in this case from Ref. [64] (here we set the density $n = 1$) and turns out to be:

$$S(k, \omega) = \frac{8|k|(k^2 + \omega)^2}{[(4k)^2 + (k^2 - \omega)^2][(4k)^2 + (k^2 + \omega)^2]}. \quad (\text{B.2})$$

so that

$$\Xi(k, \omega) = \frac{S(k, \omega) - S(k, -\omega)}{S(k, \omega) + S(k, -\omega)} = \frac{2k^2\omega}{k^4 + \omega^2}. \quad (\text{B.3})$$

Note the decay $\propto \omega^{-1}$ of $\Xi(k, \omega)$ at large ω , while one expects it to be $\propto \omega^{-2}$ in the interacting case. Replacing this expression of $\Xi(k, \omega)$ into Eq. (B.1), we obtain

$$\epsilon(\lambda) = 2 + \ln(4\lambda^2) + \text{const.}, \quad (\text{B.4})$$

where the integral was calculated with the principal value. Accordingly, by choosing

$$\text{const.} = -2 - 2 \ln 4 \quad (\text{B.5})$$

we obtain the exact GGE post-quench distribution of momenta

$$\vartheta(\lambda) = \frac{1}{1 + e^{\epsilon(\lambda)}} = \frac{1}{1 + (\lambda/2)^2} \quad (\text{B.6})$$

found in Ref. [64]. This result shows that for the $c = \infty$ case, $\beta(\lambda) = [\ln(\lambda/2)^2] / (\lambda^2 - \bar{\mu})$ and $\bar{\mu} = \epsilon(\bar{\lambda}_F = 2) = 4$.

Appendix C. The large but finite c limit

In Appendix B we considered the $c \rightarrow \infty$ limit. It is possible to develop this further and demonstrate how to extract $\vartheta(\lambda)$ from $S(k, \omega)$ up to $1/c^2$ corrections. We will demonstrate this is the case even if the momentum of the dynamic structure factor, k , is finite. This is possible because at large c the two (and greater) particle-hole contributions to $S(k, \omega)$ are suppressed by $1/c^2$ regardless of the magnitude of k . This fact was used by two of the authors here in Ref. [41] to develop an expression for $S(k, \omega)$ valid for arbitrary $\vartheta(\lambda)$ and arbitrary (k, ω) up to $1/c^2$ corrections (see Eq. (5.8) of Ref. [69])

$$S(k, \omega) = \frac{2}{\pi} \left[\pi \frac{1 + \frac{6n}{c}}{4|k|} + \frac{1}{2c} \frac{k}{|k|} \text{PV} \int_{-\infty}^{\infty} d\lambda \frac{\vartheta(\lambda + p) - \vartheta(\lambda + h)}{\lambda} \right] \vartheta(h) (1 - \vartheta(p)) + \mathcal{O}(1/c^2), \quad (\text{C.1})$$

with

$$p = \frac{k}{2(1 + 2n/c)} + \frac{\omega(1 + 2n/c)}{2k}, \quad (\text{C.2})$$

$$h = -\frac{k}{2(1 + 2n/c)} + \frac{\omega(1 + 2n/c)}{2k}. \quad (\text{C.3})$$

We see that $S(k, \omega)$ involves $\vartheta(\lambda)$ in a straightforward fashion. Even though $\vartheta(\lambda)$ appears in an integral in the above expression, we can, by using a $1/c$ expansion of ϑ ,

$$\vartheta(\lambda) = \vartheta_0(\lambda) + \frac{1}{c} \vartheta_1(\lambda) + \mathcal{O}(1/c^2), \quad (\text{C.4})$$

arrive at a simple expression for it in terms of $S(k, \omega)$. As part of this we will need to know how the $1/c$ corrections to $\omega(\lambda)$ and $k(\lambda)$ (Eqs. (16) and (15)) appear. These, however, are also straightforward to develop because the scattering kernel, $K(\lambda)$, becomes particularly simple at leading order in $1/c$:

$$K(\lambda) = \frac{2}{c} + \mathcal{O}(1/c^2). \quad (\text{C.5})$$

To proceed we first solve Eq. (C.1) for $\vartheta(\lambda)$ at leading order in $1/c$. To simplify this we consider the elastic limit, where $\omega = 0$. In this case $p = -h$ and it is straightforward to show using Eq. (C.5) that k and p are related by:

$$k = 2p(1 + 2n/c) + \mathcal{O}(1/c^2). \quad (\text{C.6})$$

In this particular case we then obtain for $\vartheta(\lambda)$

$$\vartheta(p) = \frac{1}{2} \left[1 + \sqrt{1 - 16|p|S(2p, 0)} \right] + \mathcal{O}(1/c). \quad (\text{C.7})$$

This then allows us to rewrite Eq. (C.1) as follows

$$\begin{aligned} S(k, 0) &= \frac{1}{F(k)} \vartheta(p)(1 - \vartheta(p)); \\ F^{-1}(k) &= \frac{2}{\pi} \left\{ \pi \frac{1 + \frac{6n}{c}}{4|k|} + \frac{n \operatorname{sgn}(k)}{2c} \operatorname{PV} \int_{-\infty}^{\infty} \frac{d\lambda}{\lambda} \right. \\ &\quad \left. \left[\left(1 - 16 \left| \lambda + \frac{k}{2} \right| S\left(\lambda + \frac{k}{2}, 0\right) \right)^{1/2} - \left(1 - 16 \left| \lambda - \frac{k}{2} \right| S\left(\lambda - \frac{k}{2}, 0\right) \right)^{1/2} \right] \right\}. \end{aligned} \quad (\text{C.8})$$

We can then solve this to obtain $\vartheta(\lambda)$ up to $\mathcal{O}(1/c^2)$ corrections:

$$\vartheta(p) = \frac{1}{2} \left[1 + \sqrt{1 - 4F(k)S(k, 0)} \right] \Big|_{k=2p(1+2n/c)} + \mathcal{O}(1/c^2). \quad (\text{C.9})$$

We also note that in this large c limit one can recover the same equation derived for the structure factor in Ref. [38]. In fact from Eq. (C.2) one can deduce the following properties:

$$h_{-k, \omega} = -h_{k, \omega} \quad p_{-k, \omega} = -p_{k, \omega} \quad h_{-k, -\omega} = p_{k, \omega} \quad p_{-k, -\omega} = h_{k, \omega}, \quad (\text{C.10})$$

where the subscript indicates that they are the particle and hole pair determining $S(k, \omega)$. With these properties from Eq. (C.1) one reads:

$$S(k, \omega) = S(-k, \omega), \quad \text{and} \quad \frac{S(k, \omega)}{S(-k, -\omega)} = \frac{\vartheta(h_{k, \omega})(1 - \vartheta(p_{k, \omega}))}{\vartheta(p_{k, \omega})(1 - \vartheta(h_{k, \omega}))} = e^{\epsilon(p_{k, \omega}) - \epsilon(h_{k, \omega})}, \quad (\text{C.11})$$

which gives the FDT ratio of Eq. (26) in Ref. [38]. From Eq. (39) we write:

$$\vartheta(\lambda) = \frac{1}{1 + a^{-1}(\lambda)} \quad (\text{C.12})$$

and an expansion at large c gives:

$$a^{-1}(\lambda) = \frac{\lambda^2}{4n^2} \left(1 + 4\frac{n}{c}\right) + o\left(\frac{n}{c}\right). \quad (\text{C.13})$$

Using this expression we define:

$$\bar{\lambda}_F = 2n\sqrt{\frac{c}{4n+c}} \quad \bar{\mu} = \frac{4n^2c}{4n+c} \quad \beta(\lambda) = \frac{\log a^{-1}(\lambda)}{\lambda^2 - \bar{\mu}}. \quad (\text{C.14})$$

Moreover choosing:

$$k_\lambda = \left(1 + \frac{2n}{c}\right) \left(\lambda - \frac{\bar{\mu}}{\lambda}\right) \quad \omega_\lambda = \lambda^2 - \left(\frac{\bar{\mu}}{\lambda}\right)^2 \quad (\text{C.15})$$

implies:

$$\frac{S(k_\lambda, \omega_\lambda)}{S(-k_\lambda, -\omega_\lambda)} = e^{2\epsilon(\lambda)}, \quad (\text{C.16})$$

which is a condition that directly relates the measurement of $S(k, \omega)$ to $\epsilon(\lambda)$ via the FDT (or detailed balance) ratio, in an analogous manner to what has been done in [38] for the case $c = \infty$.

Appendix D. Effects of a harmonic trap

In the previous sections we considered the case of a Bose gas in one spatial dimension and of infinite extent. However, in actual experiments, the cold atoms which constitute the gas are spatially confined by the presence of an optical trap which generates a one-body potential acting on the atoms and therefore an additional contribution $\sum_{i=1}^N V(x_i)$ in Eq. (10). This confinement typically occurs on a length scale ℓ which is large on the microscopic scale and eventually affects, e.g., the DSF $S(k, \omega)$ at small wave vectors $k \lesssim \ell^{-1}$. As Eqs. (32) and (33), which allow us to determine ϑ from $S(k, \omega)$ are actually based on its expansion at small momenta, see Eq. (30), the presence of a trap may affect significantly the whole procedure and therefore it is worth considering in more detail its effect. In particular, the trap breaks the integrability of the model, as discussed further below.

A first heuristic estimate of the consequences of a trap can be obtained by considering the static structure factor

$$S(k) \equiv \int_{-\infty}^{\infty} \frac{d\omega}{2\pi} S(k, \omega), \quad (\text{D.1})$$

in the ground state of the gas, as opposed to its dynamical counterpart $S(k, \omega)$. The effects on measuring $S(k)$ after release from a trap was computed in Ref. [69], where it was argued that a harmonic trap $V(x) = m\omega_{\text{trap}}^2 x^2/2$ (where m is the mass of the gas particles) of characteristic frequency ω_{trap} changes the structure factor S by an amount δS which, at small momenta reads [69]

$$\delta S(k \ll k_F) = \frac{k_F}{16\pi} \left(\frac{\omega_{\text{trap}}}{\epsilon_F}\right)^4 \left(\frac{k_F}{k}\right)^5, \quad (\text{D.2})$$

with the Fermi energy given by $\epsilon_F = k_F^2$. The dependence of δS on k^{-5} seemingly suggests that the actual structure factor in the presence of the trap is significantly affected at small wave vectors compared to the one in its absence. However, under actual reported experimental conditions [43], the correction implied by Eq. (D.2) is actually small even for $k_{\text{trap}} = 2\pi/L_{\text{trap}} \sim \frac{\epsilon_F}{\pi\omega}$ where L_{trap} is the length of the trap. Ref. [43] reported $\omega_{\text{trap}}/\epsilon_F \sim 10^{-2}$. In this case $\delta S(k_{\text{trap}}) \sim 10^{-4}k_F$.

A second characterization of the trap can be made using the local density approximation (LDA). The LDA as applied to the determination of the DSF, tells us that the measured $S(k, \omega)$ in a trap should be averaged over the spatial extent of the trap, i.e.

$$S_{\text{measured}}(k, \omega) = \int_{-L_{\text{trap}}/2}^{L_{\text{trap}}/2} dx S(k, \omega, n(x)), \quad (\text{D.3})$$

where $n(x)$ is the density of the gas at position x of the trap. The density at a given point is given by

$$n(x) = \frac{1}{\sqrt{\pi}} \left(\pi n_0^2 - \frac{\omega_{\text{trap}}^2 x^2}{4} \right)^{1/2}. \quad (\text{D.4})$$

where $n_0 = n(0)$ is the density at the center of the trap and ω_{trap} is the strength of the trap. This allows us to recast S_{measured} in a simple form,

$$S_{\text{measured}}(k, \omega) = \int_0^1 dy \frac{y}{\sqrt{1-y^2}} S(k, \omega, n_0 y). \quad (\text{D.5})$$

Note that ω_{trap} does not directly appear in this expression.

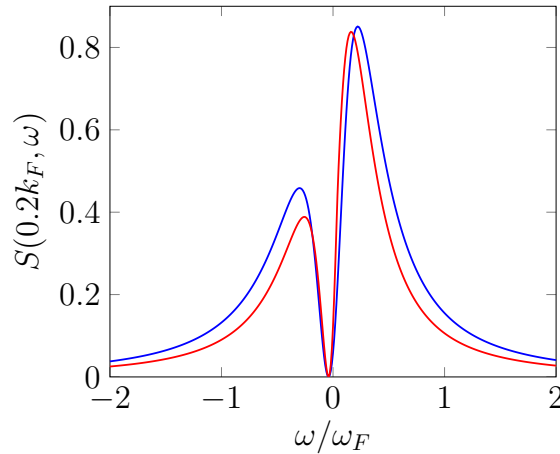


Figure D1. Plot of $S(k, \omega)$ at density $n = k_F/\pi$ in a homogeneous system (blue line) against $S(k, \omega)$ in a trap as computed using the LDA (red line). We see that while the trap effects small quantitative changes on $S(k, \omega)$, it leaves the overall line shape intact.

Using Eq. (D.5), we can see how the trap distorts the DSF $S(k, \omega)$. As an example, we explicitly consider the $c = \infty$ case where from Ref. [64] we have an exact expression

for the DSF as a function of density:

$$S(k, \omega, n) = \frac{8n^2(k^2 + \omega)|k|}{((4nk)^2 + (k^2 - \omega)^2)((4nk)^2 + (k^2 + \omega)^2)}. \quad (\text{D.6})$$

Using this expression, in Fig. D1 we plot both $S(k, \omega, n_0)$ as well as $S_{\text{measured}}(k, \omega)$. We see that while there are distortions to $S(k, \omega)$ induced by the trap, they are relatively small. Unlike the zero temperature case [70, 71], the change in lineshape of the DSF is quantitative, not qualitative.

Beyond the issue of the extent that the trap distorts the dynamic structure function, its presence gives rise to the need to address how exactly the late time dynamics of the gas is still described by a GGE, the premise of this paper. In part this is a question of time scales and strength of the integrability breaking. The integrability breaking due to the trap happens on a certain time scale, τ_{break} . Provided this time scale is much longer than the time scale, τ_{rel} , governing relaxation in the system, i.e., $\tau_{\text{break}} \gg \tau_{\text{rel}}$, we can expect the system to relax to what is known to an ensemble governed by a deformed GGE (see Refs. [72, 73]). A deformed GGE is an ensemble that still possesses an infinite number of charges, but whose charges differ (parametrically in the strength of the integrability breaking) from the original. But this means that we can conclude provided integrability breaking is sufficiently weak that we expect that a time range emerges within which $S(k, \omega)$ is well described by the GGE of the original, unperturbed, model. This plateau is known typically as a prethermalization plateau [31, 74, 75].

The discussion in the previous paragraph assumed that the system was in the thermodynamic limit. However we can ask the same question on the fate of the GGE in a *finite* system (as all experimental systems are), namely does weak integrability breaking due to a trap lead to relaxation to a state governed by a Gibbs ensemble (at least up to finite-size corrections)? Here the answer is that even at infinite time, weak integrability breaking may not lead to Gibbs-like thermalization. As shown in [28], a remnant of the conserved charges survive integrability breaking (in the same spirit that integrability breaking in a classical integrable system does not destroy all invariant tori). These remnants will prevent the system from ever thermalizing to a Gibbs ensemble and might be thought of as the infinitely long-lived relatives of the deformed GGE described in Refs. [72, 73]).

Appendix E. Discussion on possible experimental realizations

In this section we discuss the feasibility of an experimental realization of the proposed method of determining the GGE state. The current experimental techniques allow one to realize the one-dimensional Bose gas either in the atom chip setup [56, 76] or through optical lattices [77–79]. In the latter, the one-dimensional Bose gas is created by tightly confining the motion of the cloud of atoms to a single direction. The periodicity of the optical lattice results not in a single one-dimensional Bose gas, but in an two-dimensional array of “one-dimensional tubes” (see Fig. E1). A gas in each tube is

effectively described by the Lieb-Liniger model but with different densities, maximal in the center of the array and decreasing outwards. This has two effects. First, the effective interaction parameter $\gamma = c/n$ varies among the array. The tubes further from the center have stronger interactions. Second, it affects the Bragg spectroscopy. Let us discuss the second effect in a greater detail.

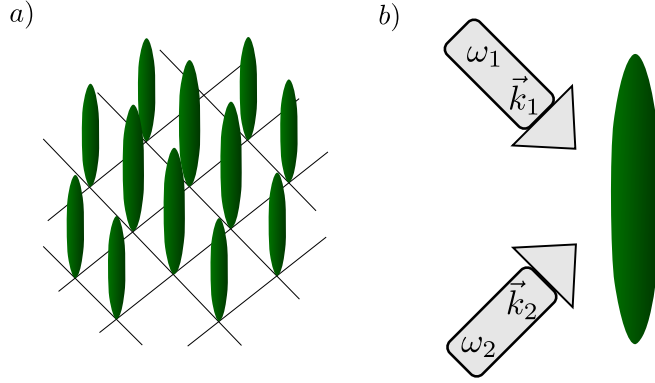


Figure E1. a) The 2d optical lattice creates an array of 1d tubes. b) The Bragg scattering perturbs the gas in each tube with energy $\omega = \omega_1 - \omega_2$ and momentum k proportional to the magnitude of $|\vec{k}_1| = |\vec{k}_2|$ and depending on the relative angle between them. The above image is reproduced from [44].

In the Bragg spectroscopy experiments [43, 44, 57, 80] two slightly detuned lasers created a standing wave which perturbs the gas, c.f. Fig. E1. The momentum k of the perturbation depends on the geometry, while the energy ω on the detuning. Taking the relatively small size of the array of the atoms into account we can safely assume that k is constant throughout the array. Therefore each tube is perturbed with the same momentum and energy. However the gas in the tubes further from the center has lower density, therefore effectively it is perturbed at higher momentum (recall that $k_F = \pi n$). This has the following consequences.

Let us setup the experiment in such a way that the center tubes are perturbed at small momenta (with respect to their k_F). This gives $S(k, \omega)$ at small k which is exactly what we need to recover the distribution $\vartheta(\lambda)$. However the tubes further from the center will be perturbed at higher momenta and it seems that we could not determine $\vartheta(\lambda)$ from their DSF. Fortunately, the interactions in these tubes are also stronger, their γ is larger. Therefore what we obtain from the Bragg spectroscopy is a DSF at larger momenta of a stronger interacting one-dimensional Bose gas. It turns out that for a strongly interacting gas we can use a slightly different method of determining $\vartheta(\lambda)$. It is based on the perturbative expansion around $\gamma = \infty$ and in Appendix C we provide the details.

What is important is that both methods of determining the $\vartheta(\lambda)$ are complementary. One, the focus of this work, relies on small k features of the DSF and is valid for all interaction strengths. The second, based on a $1/\gamma$ expansion, is valid only for strong enough interactions (values of $\gamma > 10$ usually prove to be enough), but

does not place any restriction on the momentum of the DSF. This allows us to cover the whole variety of physical situations encountered in the Bragg spectroscopy of the one-dimensional Bose gas created in optical lattices.

Finally let us also mention the relevant timescales. In an experimental setting we would imagine measuring the Bragg spectra at various times after the quench and averaging them according to Eq. (37). An important assumption hidden behind these considerations is that the time of the Bragg pulse is much shorter than a characteristic time of the quench dynamics. This is usually the case as $\omega_{\text{Bragg}} \sim \epsilon_F \sim 10^4 \text{s}^{-1}$ (see, e.g., Ref. [44]) while $\omega_{\text{relaxation}} \sim 1 \text{s}^{-1}$ (see, e.g., Ref. [30]).

Appendix F. Few words on the numerical evaluation of the dynamic structure factor

The ABACUS [46] software package evaluates the DSF for a fixed number of particles N and finite length of the system L . From this finite size data we can infer the shape of the function in the thermodynamic limit. In Fig. F1 we check the dependence of the results on the number of particles N (recall that we always work with a fixed density $n = N/L = 1$). The results show that the finite-size effects are small (order of 10^{-2}).

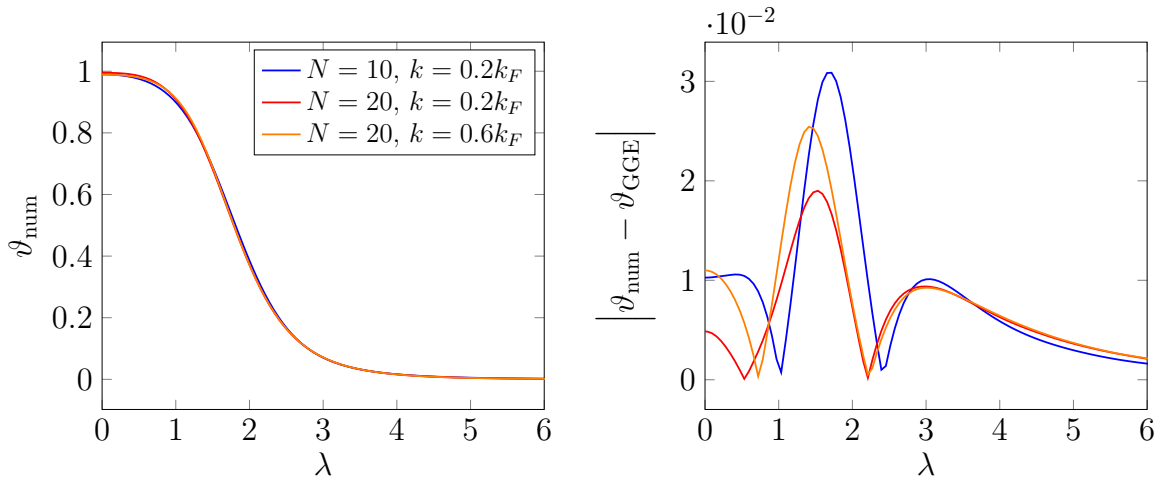


Figure F1. Left panel: Comparison between the distributions ϑ_{num} obtained from the Bragg spectra measured at different system sizes $N = 10$ and $N = 20$ and different momenta $k = 0.2 k_F$ and $k = 0.6 k_F$, in the quench $c = 0 \rightarrow c = 2$. Right panel: plot of the difference between the numerically computed ϑ_{num} (with the same system sizes N and momenta k as in the left panel) and the exact distribution ϑ_{GGE} . We notice that larger system sizes N and smaller momentum k give a more accurate prediction for $\vartheta(\lambda)$ around $\lambda \sim 0$, while deviations in the tails remain relatively large due to the numerically truncated diagonal ensemble sum (38).

The DSF $S(k, \omega)$ determined with ABACUS is a set of equally distributed discrete set of points in k (quantized as $2\pi I/L$ with integer I) and unequally distributed points in the ω variable. In order to take the ratio in the definition of the $\Xi(k, \omega)$ we smoothen

the DSF in ω by convoluting it with a Gaussian function with width $\sigma = w\Delta E$ and $w = 0.1$ or 0.5 and with ΔE the two-particle level spacing, and evaluating it on an equally distributed set of points in ω . We have verified that this smoothening procedure does not affect the results.

References

- [1] Polkovnikov A, Sengupta K, Silva A and Vengalattore M 2011 *Rev. Mod. Phys.* **83** 863
- [2] Calabrese P 2016 *J. Stat. Mech.* 064001
- [3] Gogolin C and Eisert J 2016 *Rep. Prog. Phys.* **79** 056001
- [4] Kinoshita T, Wenger T and Weiss D S 2006 *Nature* **440** 900
- [5] Hofferberth S, Lesanovsky I, Fischer B, Schumm T and Schmiedmayer J 2007 *Nature* **449** 324
- [6] Bloch I, Dalibard J and Zwerger W 2008 *Rev. Mod. Phys.* **80** 885
- [7] Trotzky S, Chen Y A, Flesch A, McCulloch I P, Schollwöck U, Eisert J and Bloch I 2012 *Nat. Phys.* **8** 325
- [8] Cheneau M, Barmettler P, Poletti D, Endres M, Schauss P, Fukuhara T, Gross C, Bloch I, Kollath C and Kuhr S 2012 *Nature* **481** 484
- [9] Langen T, Erne S, Geiger R, Rauer B, Schweigler T, Kuhnert M, Rohringer W, Mazets I E, Gasenzer T and Schmiedmayer J 2015 *Science* **348** 207–211
- [10] Rigol M, Dunjko V, Yurovsky V and Olshanii M 2007 *Phys. Rev. Lett.* **98** 050405
- [11] Rigol M, Dunjko V and Olshanii M 2008 *Nature* **452** 854
- [12] Calabrese P, Essler F H L and Fagotti M 2011 *Phys. Rev. Lett.* **106**(22) 227203
- [13] Foini L, Cugliandolo L F and Gambassi A 2011 *Phys. Rev. B* **84** 212404
- [14] Fioretto D and Mussardo G 2010 *New J. Phys.* **12** 055015
- [15] Mossel J and Caux J S 2012 *J. Phys. A: Math. Theor.* **45** 255001
- [16] Pozsgay B 2013 *J. Stat. Mech. Theor. Exp.* P07003
- [17] Wouters B, De Nardis J, Brockmann M, Fioretto D, Rigol M and Caux J S 2014 *Phys. Rev. Lett.* **113**(11) 117202
- [18] Pozsgay B, Mestyán M, Werner M A, Kormos M, Zaránd G and Takács G 2014 *Phys. Rev. Lett.* **113**(11) 117203
- [19] Ilievski E, De Nardis J, Wouters B, Caux J S, Essler F H and Prosen T 2015 *Phys. Rev. Lett.* **115** 157201
- [20] Ilievski E, Quinn E, De Nardis J and Brockmann M 2016 *J. Stat. Mech. Theor. Exp* **2016** 063101
- [21] Vernier E and Cubero A C 2017 *J. Stat. Mech. Theor. Exp* **2017** 023101
- [22] Vidmar L and Rigol M 2016 *J. Stat. Mech. Theor. Exp* **2016** 064007
- [23] Essler F H L, Evangelisti S and Fagotti M 2012 *Phys. Rev. Lett.* **109**(24) 247206
- [24] De Luca A, Collura M and De Nardis J arXiv:1612.07265
- [25] B Pozsgay E Vernier M W 2017 arXiv:1703.09516
- [26] Marino J and Silva A 2012 *Phys. Rev. B* **86**(6) 060408
- [27] Fagotti M 2014 *J. Stat. Mech. Theor. Exp.* **2014** P03016
- [28] Brandino G P, Caux J S and Konik R M 2015 *Phys. Rev. X* **5**(4) 041043
- [29] Bertini B, Essler F H L, Groha S and Robinson N J 2015 *Phys. Rev. Lett.* **115**(18) 180601
- [30] van den Berg R, Wouters B, Eliëns S, De Nardis J, Konik R M and Caux J S 2016 *Phys. Rev. Lett.* **116**(22) 225302
- [31] Marcuzzi M, Marino J, Gambassi A and Silva A 2013 *Phys. Rev. Lett.* **111** 197203
- [32] Deutsch J M 1991 *Phys. Rev. A* **43**(4) 2046–2049
- [33] Srednicki M 1994 *Phys. Rev. E* **50**(2) 888–901
- [34] Kubo R 1966 *Rep. Prog. Phys.* **29** 255
- [35] Cugliandolo L F, Kurchan J and Peliti L 1997 *Phys. Rev. E* **55** 3898
- [36] Cugliandolo L F 2011 *J. Phys. A* **44** 483001
- [37] Foini L, Cugliandolo L F and Gambassi A 2012 *J. Stat. Mech.* **P09011**
- [38] Foini L, Gambassi A, Konik R and Cugliandolo L F arXiv:1610.00101
- [39] Lieb E H and Liniger W 1963 *Phys. Rev.* **130** 1605
- [40] Lieb E H 1963 *Phys. Rev.* **130** 1616
- [41] De Nardis J and Panfil M 2016 *SciPost Phys.* **1**(2) 015
- [42] De Nardis J and Panfil M 2015 *J. Stat. Mech. Theor. Exp* **2015** P02019

- [43] Fabbri N, Panfil M, Clément D, Fallani L, Inguscio M, Fort C and Caux J S 2015 *Phys. Rev. A* **91**(4) 043617
- [44] Meinert F, Panfil M, Mark M J, Lauber K, Caux J S and Nägerl H C 2015 *Phys. Rev. Lett.* **115**(8) 085301
- [45] Sotiriadis S and Calabrese P 2014 *J. Stat. Mech. Theor. Exp* **2014** P07024
- [46] Caux J S 2009 *J. Math. Phys.* **50** 095214
- [47] Korepin V E, Bogoliubov N M and Izergin A G 1993 *Quantum Inverse Scattering Method and Correlation Functions* (Cambridge: Cambridge Univ. Press)
- [48] Kormos M, Shashi A, Chou Y Z, Caux J S and Imambekov A 2013 *Phys. Rev. B* **88**(20) 205131
- [49] De Nardis J, Wouters B, Brockmann M and Caux J S 2014 *Phys. Rev. A* **89** 033601
- [50] Essler F H L, Mussardo G and Panfil M 2015 *Phys. Rev. A* **91**(5) 051602
- [51] Essler F H L, Mussardo G and Panfil M 2017 *J. Stat. Mech. Theor. Exp* **2017** 013103
- [52] Caux J S and Essler F H L 2013 *Phys. Rev. Lett.* **110**(25) 257203
- [53] Cassidy A C, Clark C W and Rigol M 2011 *Phys. Rev. Lett.* **106**(14) 140405
- [54] Ilievski E, Quinn E and Caux J S 2017 *Phys. Rev. B* **95**(11) 115128
- [55] De Nardis J, Piroli L and Caux J S 2015 *J. Phys. A: Math. Theor.* **48** 43FT01
- [56] van Amerongen A H, van Es J J P, Wicke P, Kheruntsyan K V and van Druten N J 2008 *Phys. Rev. Lett.* **100** 090402
- [57] Fabbri N, Clément D, Fallani L, Fort C and Inguscio M 2011 *Phys. Rev. A* **83**(3) 031604
- [58] Paredes B, Widera A, Murg V, Mandel O, Fölling S, Cirac I, Shlyapnikov G V, Hänsch T W and Bloch I 2004 *Nature* **429** 277
- [59] Cugliandolo L F and Lozano G S 1998 *Phys. Rev. Lett.* **80** 4979
- [60] De Nardis J, Wouters B, Brockmann M and Caux J S 2014 *Phys. Rev. A* **89**(3) 033601
- [61] Caux J S and Maillet J M 2005 *Phys. Rev. Lett.* **95** 077201
- [62] Caux J S and Calabrese P 2006 *Phys. Rev. A* **74** 031605
- [63] Panfil M and Caux J S 2014 *Phys. Rev. A* **89**(3) 033605
- [64] Kormos M, Collura M and Calabrese P 2014 *Phys. Rev. A* **89**(1) 013609
- [65] Bertini B, Collura M, De Nardis J and Fagotti M 2016 *Phys. Rev. Lett.* **117**(20) 207201
- [66] Castro-Alvaredo O A, Doyon B and Yoshimura T 2016 *Phys. Rev. X* **6**(4) 041065
- [67] Mussardo G 2010 *Statistical Field Theory* (Oxford University Press)
- [68] Mussardo G 2013 *Phys. Rev. Lett.* **111**(10) 100401
- [69] Caux J S and Konik R M 2012 *Phys. Rev. Lett.* **109**(17) 175301
- [70] Golovach V N, Minguzzi A and Glazman L I 2009 *Physical Review A* **80** 043611
- [71] Vignolo P, Minguzzi A and Tosi M P 2001 *Phys. Rev. A* **64**(2) 023421
- [72] Essler F H L, Kehrein S, Manmana S R and Robinson N J 2014 *Phys. Rev. B* **89**(16) 165104
- [73] Bertini B, Essler F H L, Groha S and Robinson N J 2016 *Phys. Rev. B* **94**(24) 245117
- [74] Moeckel M and Kehrein S 2008 *Phys. Rev. Lett.* **100**(17) 175702
- [75] Langen T, Gasenzer T and Schmiedmayer J 2016 *J. Stat. Mech. Theor. Exp* **2016** 064009
- [76] Hofferberth S, Lesanovsky I, Schumm T, Imambekov A, Gritsev V, Demler E and Schmiedmayer J 2008 *Nat. Phys.* **4** 489
- [77] Kinoshita T, Wenger T and Weiss D S 2004 *Science* **305** 1125–1128
- [78] Kinoshita T, Wenger T and Weiss D S 2005 *Phys. Rev. Lett.* **95** 190406
- [79] Haller E, Gustavsson M, Mark M J, Danzl J G, Hart R, Pupillo G and Nägerl H C 2009 *Science* **325** 1224–1227
- [80] Brunello A, Dalfovo F, Pitaevskii L, Stringari S and Zambelli F 2001 *Phys. Rev. A* **64**(6) 063614